Supplementary Materials for: Effect of particle size on thermodynamics and lithium ion transport in electrodes made of $Ti_2Nb_2O_9$ microparticles or nanoparticles

Yucheng Zhou[a], Etienne Le Calvez[b,c], Sun Woong Baek[a], Matevž Frajnkovič[a], Camille Douard[b,c], Eric Gautron[b], Olivier Crosnier[b,c], Thierry Brousse[b,c], and Laurent Pilon[a,d,e,+]

[a]Mechanical and Aerospace Engineering Department, Henry Samueli School of Engineering and Applied Science, University of California, Los Angeles, CA 90095, USA

[b]Nantes Université, CNRS, Institut des Matériaux de Nantes Jean Rouxel, IMN, F-44000 Nantes, France

[c]Réseau sur le Stockage Électrochimique de l'Énergie (RS2E), CNRS FR 3459, 33 rue Saint Leu, 80039 Amiens Cedex, France

[d]California NanoSystems Institute, University of California, Los Angeles, CA 90095, USA

[e]Institute of the Environment and Sustainability, University of California, Los Angeles, CA 90095, USA

[+]Corresponding Author: Phone: +1 (310)-206-5598, Fax: +1 (310)-206-2302

E-mail: pilon@seas.ucla.edu

July 4, 2022

S.1 Structural characterization

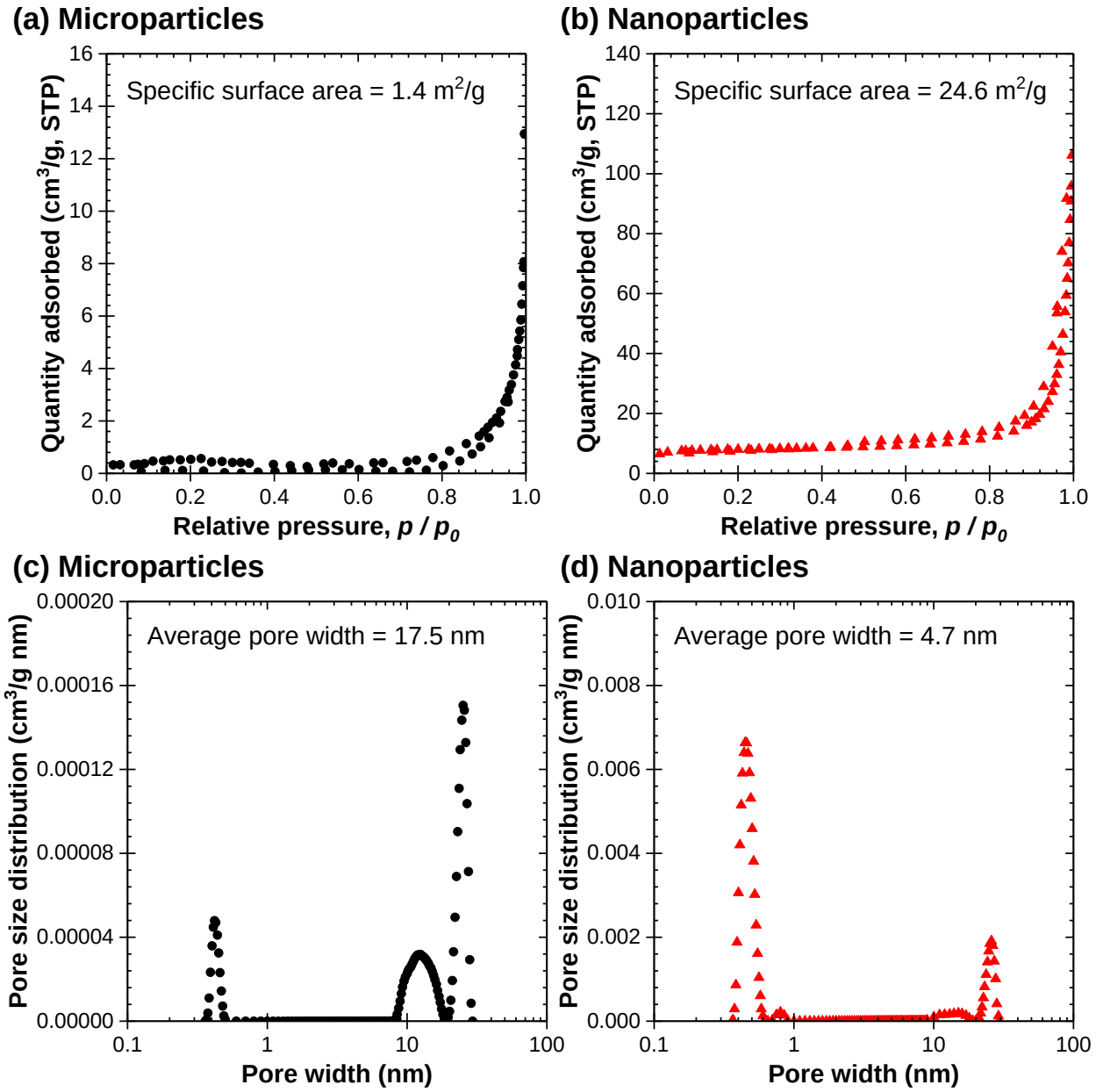

Figure S1: Quantity adsorbed as a function of relative pressure p/p_0 in low-temperature nitrogen adsorption porosimetry of $Ti_2Nb_2O_9$ (a) microparticles or (b) nanoparticles. Pore size distribution as a function of pore width in low-temperature nitrogen adsorption porosimetry of $Ti_2Nb_2O_9$ (c) microparticles or (d) nanoparticles.

S.2 *Operando* isothermal calorimetry

S.2.1 Cell potential

Figure S2 plots the temporal evolution of the potential $V(t)$ of the calorimetric cells with slurry-cast working electrodes made of $Ti_2Nb_2O_9$ (a) microparticles or (b) nanoparticles and lithium metal counter electrodes for six consecutive galvanostatic cycles with potential window between 1.0 and 3.0 V vs. Li/Li^+ for each current I ranging from 2 to 8 mA. Here, the five colored regions corresponded to the different current I from 2 to 4 to 6 to 8 and back to 2 mA. The $Ti_2Nb_2O_9$ active material mass loading of both cells was identical at 5.5 mg, such that identical currents I would result in identical C-rates. The current $I = 2$, 4, 6, and 8 mA amounted to C-rate of 1.5C, 3C, 4.5C, and 6C, respectively. Furthermore, the potential $V(t)$ of both cells was nonlinear and asymmetric between charging and discharging. This followed the typical potential profiles under galvanostatic cycling. In addition, the potential $V(t)$ was repeatable between every cycle for any given current I.

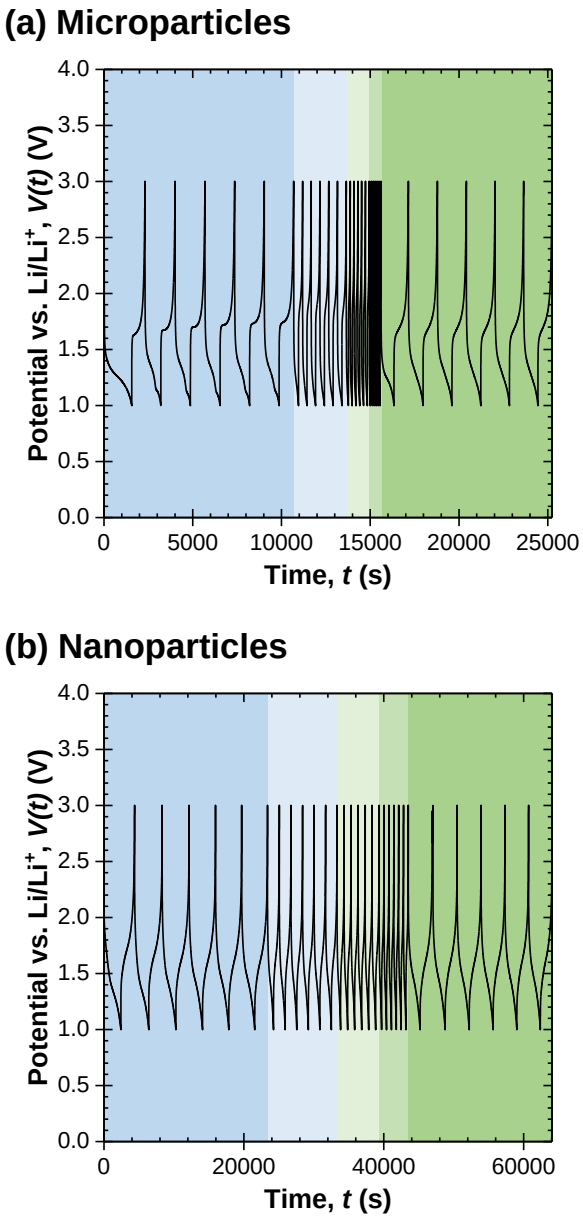

Figure S2: Temporal evolution of potential $V(t)$ of calorimetric cells for six consecutive galvanostatic cycles with potential window between 1.0 and 3.0 V vs. Li/Li^+ for each current I ranging from 2 to 8 mA with slurry-cast working electrodes made of $Ti_2Nb_2O_9$ (a) microparticles or (b) nanoparticles and lithium metal counter electrodes.

S.2.2 Instantaneous heat generation rates

Figures S3 and S4 plot the instantaneous heat generation rates $\dot{Q}_{TNO}(t)$ measured at the working electrodes made of $Ti_2Nb_2O_9$ microparticles or nanoparticles and $\dot{Q}_{Li}(t)$ measured at the lithium metal counter electrodes as functions of dimensionless time t/t_{cd} during the last three consecutive cycles at current (a) $I = 2$ mA, (b) $I = 4$ mA, (c) $I = 6$ mA, and (d) $I = 8$ mA. Here, $\dot{Q}_{TNO}(t)$ and $\dot{Q}_{Li}(t)$ in both cells showed negligible differences at any given current I. This indicates that heat generation had reached oscillatory steady-state after the first three consecutive cycles.

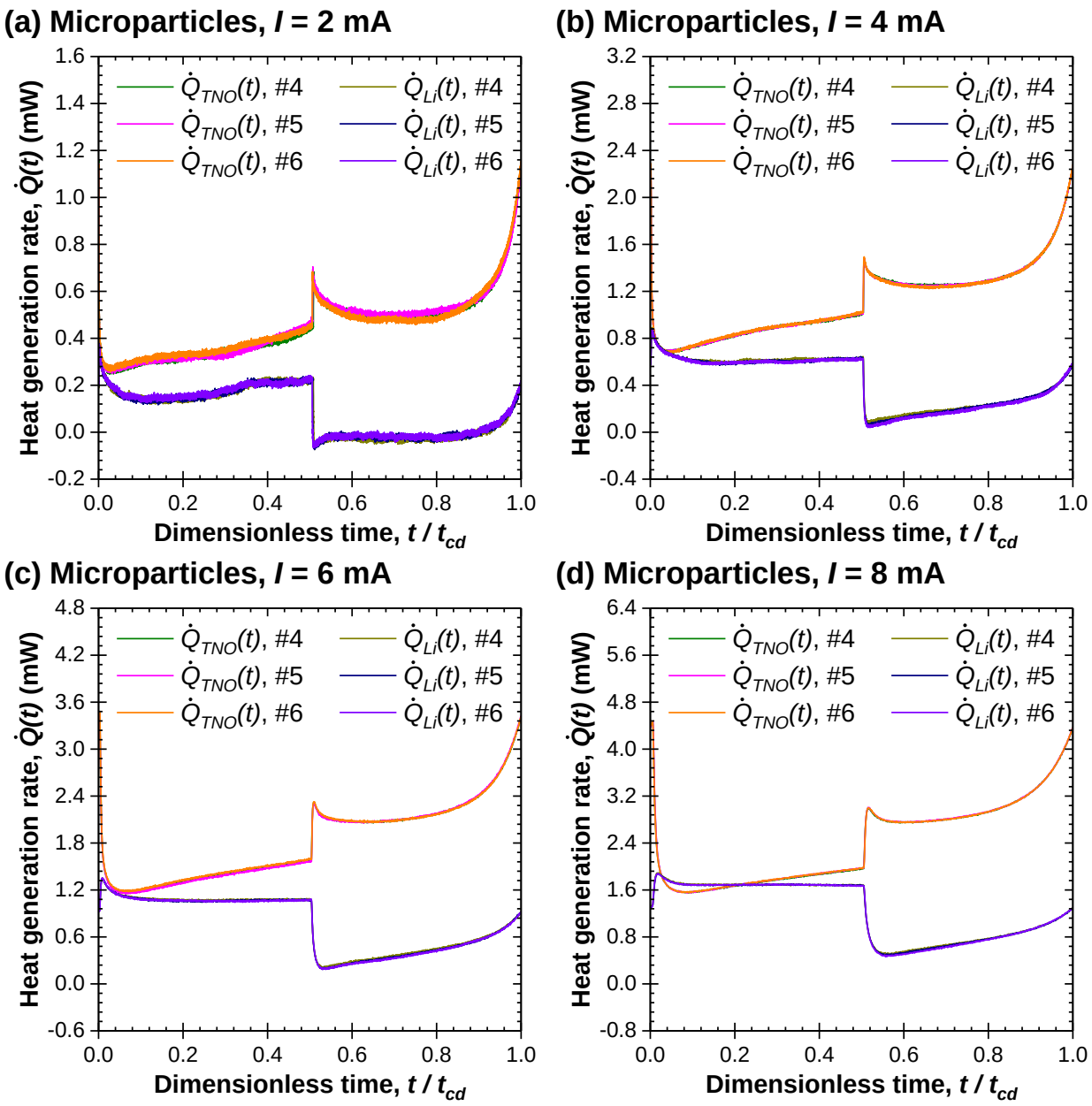

Figure S3: Instantaneous heat generation rates $\dot{Q}_{TNO}(t)$ measured at the working electrode made of $Ti_2Nb_2O_9$ microparticles and $\dot{Q}_{Li}(t)$ measured at the lithium metal counter electrode as functions of dimensionless time t/t_{cd} during the last three consecutive cycles at current (a) $I = 2$ mA, (b) $I = 4$ mA, (c) $I = 6$ mA, and (d) $I = 8$ mA.

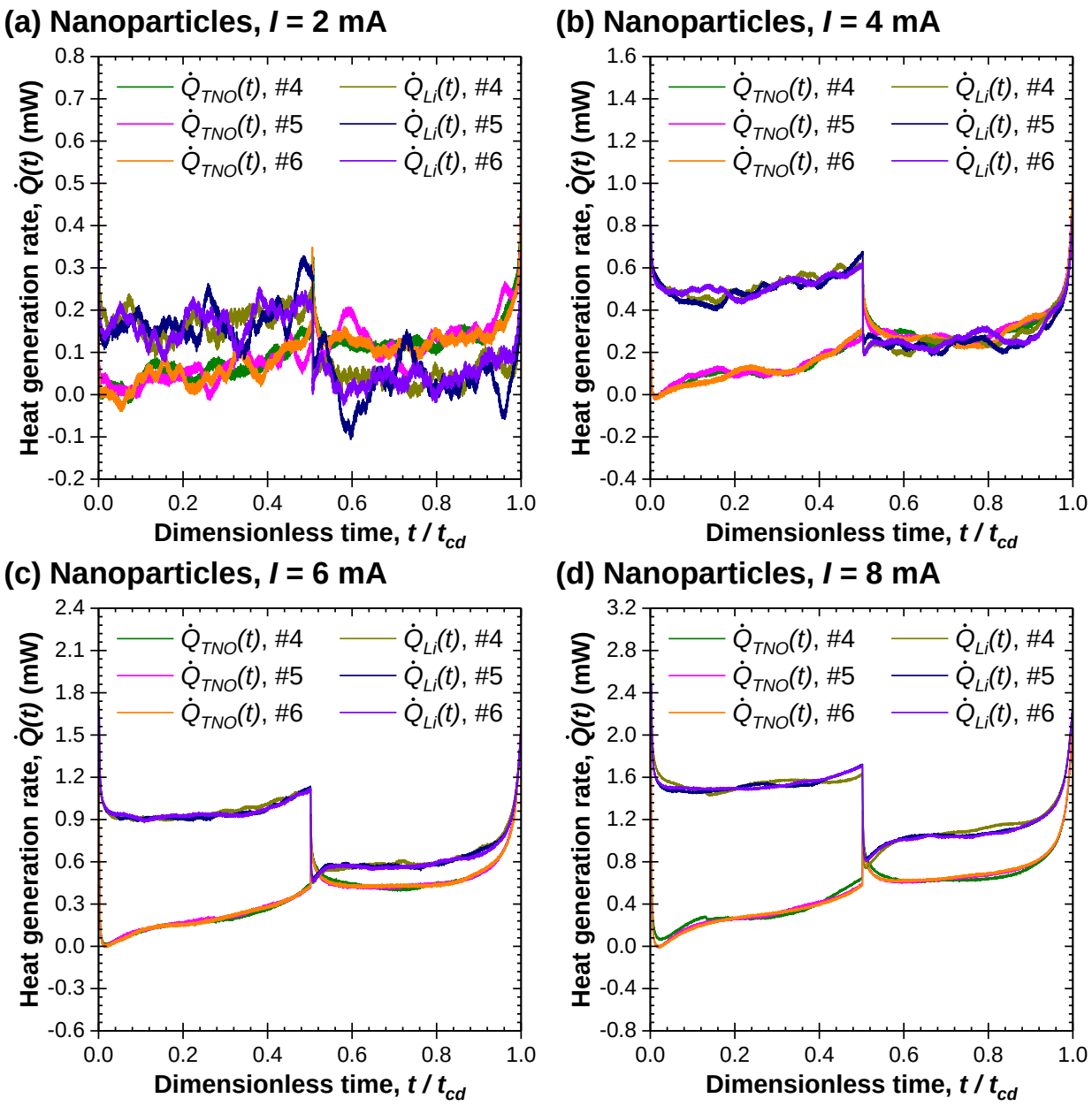

Figure S4: Instantaneous heat generation rates $\dot{Q}_{TNO}(t)$ measured at the working electrode made of $Ti_2Nb_2O_9$ nanoparticles and $\dot{Q}_{Li}(t)$ measured at the lithium metal counter electrode as functions of dimensionless time t/t_{cd} during the last three consecutive cycles at current (a) $I = 2$ mA, (b) $I = 4$ mA, (c) $I = 6$ mA, and (d) $I = 8$ mA.

S.2.3 Total heat generation rate of the cell

Figure S5 plots the open-circuit voltage $U_{OCV}(C_m, T)$ and entropic potential $\partial U_{OCV}(C_m, T)/\partial T$ of the coin cells with slurry-cast working electrodes made of $Ti_2Nb_2O_9$ microparticles or nanoparticles as functions of specific capacity C_m during lithiation and delithiation of the first cycle at C-rates of 1.5C and 6C. Here, the values of $U_{OCV}(C_m, T)$ and $\partial U_{OCV}(C_m, T)/\partial T$ measured at 1.5C were used as the values of $U^{avg}(x, T)$ and $\partial U^{avg}(x, T)/\partial T$ in Equations (5) and (6) in Manuscript for both $I = 2$ and 4 mA, while those measured at 6C were used for both $I = 6$ and 8 mA. Note that the conversion between specific capacity C_m and lithium composition x was performed such that the theoretical specific capacity of 252 mAh/g corresponded to 4 units of lithium ion insertion per unit of $Ti_2Nb_2O_9$. Thus, Figures S6 to S9 plot the measured total heat generation rate $\dot{Q}_T(x, T)$ in the calorimetric cells with slurry-cast working electrodes made of $Ti_2Nb_2O_9$ microparticles or nanoparticles and lithium metal counter electrodes as a function of lithium composition x during lithiation or delithiation for current I ranging from 2 to 8 mA. The figures also show the heat generation rates $\dot{Q}_J(x, T)$ and $\dot{Q}_J(x, T) + \dot{Q}_{rev}(x, T)$ calculated according to Equations (5) and (6) in Manuscript. Previously in cells with $TiNb_2O_7$ [1] or PNb_9O_{25} [2] working electrodes and lithium metal counter electrodes in 1 M $LiPF_6$ in EC:DMC 1:1 v/v electrolyte, the measured heat generation rate $\dot{Q}_T(x, T)$ agreed relatively well with that calculated as $\dot{Q}_J(x, T) + \dot{Q}_{rev}(x, T)$, with the difference attributed to heat of mixing $\dot{Q}_{mix}(x, T)$ [2]. Here however, major discrepancies were observed between the measurements of $\dot{Q}_T(x, T)$ and the calculations of $\dot{Q}_J(x, T) + \dot{Q}_{rev}(x, T)$ for nearly every current I in both cells. Moreover, for significant portions of the lithiation or delithiation steps, the calculated Joule heating $\dot{Q}_J(x, T)$ was negative.

Here, we hypothesize that the problem arose from limitations in the analysis. Specifically, the analysis is formulated upon the following assumption: the $U^{avg}(x, T)$ and $\partial U^{avg}(x, T)/\partial T$ in Equations (5) and (6) in Manuscript are equivalent to the $U_{OCV}(x, T)$ and $\partial U_{OCV}(x, T)/\partial T$ obtained from potentiometric entropy measurements but for current pulses corresponding to the same C-rate as that imposed during galvanostatic cycling in the *operando* isothermal

calorimetry measurements of $\dot{Q}_T(x,T)$ [2]. However, this assumption could be invalid in some circumstances. For example, for the cell with $Ti_2Nb_2O_9$ microparticles, a specific capacity of $C_m = 203$ mAh/g was extracted during lithiation under potentiometric entropy measurements with current pulses at 6C [Figure S5(a)]. By contrast, during lithiation under galvanostatic cycling at $I = 8$ mA (∼6C), the lithium composition varied from $x = 1.8$ to $x = 2.2$ corresponding to a specific capacity of $C_m = 25$ mAh/g only [Figure S7(c)]. Meanwhile, a specific capacity of $C_m = 254$ mAh/g with current pulses at 1.5C [Figure S5(a)] did not agree either with a specific capacity of $C_m = 82$ mAh/g from $x = 1.6$ to $x = 2.9$ obtained at $I = 2$ mA (∼1.5C) [Figure S6(a)]. Similar behavior was observed for the cell with $Ti_2Nb_2O_9$ nanoparticles: $C_m = 270$ mAh/g at 6C [Figure S5(c)] against $C_m = 139$ mAh/g from $x = 1.5$ to $x = 3.7$ at $I = 8$ mA (∼6C) [Figure S9(c)], or $C_m = 314$ mAh/g at 1.5C [Figure S5(c)] against $C_m = 189$ mAh/g from $x = 1.2$ to $x = 4.2$ at $I = 2$ mA (∼1.5C) [Figure S8(a)]. These comparisons suggest that the actual $U^{avg}(x,T)$ and $\partial U^{avg}(x,T)/\partial T$ reached under galvanostatic cycling did not equate to the $U_{OCV}(x,T)$ and $\partial U_{OCV}(x,T)/\partial T$ determined by potentiometric entropy measurements, otherwise the specific capacity C_m from the two measurements at the same C-rate should be much closer. In fact, the discrepancy was more significant at higher C-rates when the capacity retention was the worst. Most likely, the long relaxation periods required in potentiometric entropy measurements mitigated some dynamic processes occurring in the cell. For instance, the ion concentration gradients had time to decay, the lattice displacements had time to recover, the intercalated lithium ions had time to migrate towards more energetically favorable sites. It is interesting to note that, while previous studies did achieve good agreement between the measured $\dot{Q}_T(x,T)$ and the calculated $\dot{Q}_J(x,T) + \dot{Q}_{rev}(x,T)$ heat generation rates in cells with $TiNb_2O_7$ [1] or PNb_9O_{25} [2] working electrodes, the cells were only cycled at C-rates with good capacity retention. Therefore, the specific capacity C_m from potentiometric entropy measurements and galvanostatic cycling at the same C-rates were relatively close. As a result, in such cases the $U^{avg}(x,T)$ and $\partial U^{avg}(x,T)/\partial T$ in Equations (5) and (6) in Manuscript could be substituted with the measured $U_{OCV}(x,T)$ and $\partial U_{OCV}(x,T)/\partial T$.

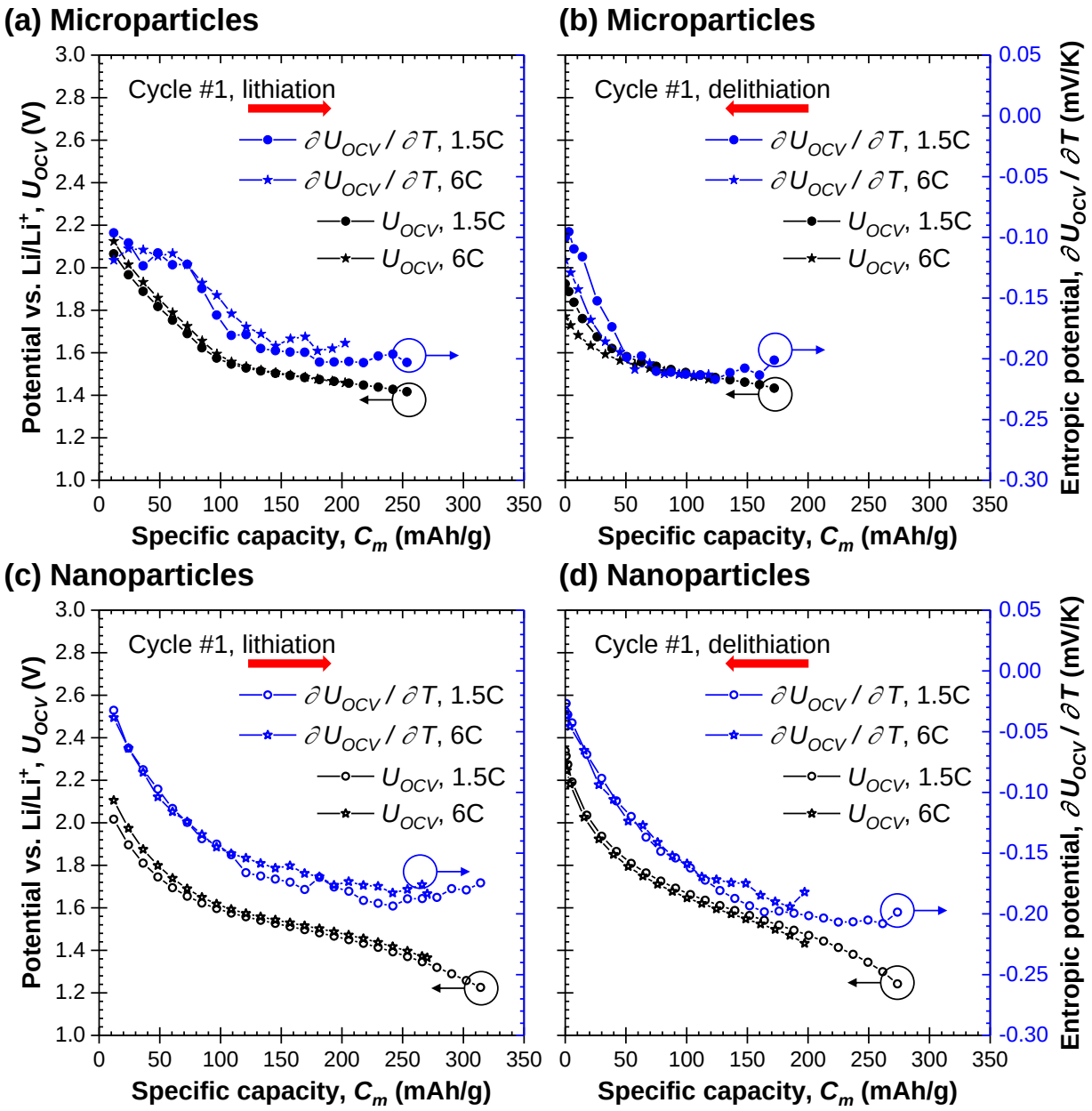

Figure S5: Open-circuit voltage $U_{OCV}(C_m, T)$ and entropic potential $\partial U_{OCV}(C_m, T)/\partial T$ of coin cells with working electrodes made of $Ti_2Nb_2O_9$ microparticles or nanoparticles as functions of specific capacity C_m during lithiation and delithiation of the first cycle at C-rates of 1.5C and 6C.

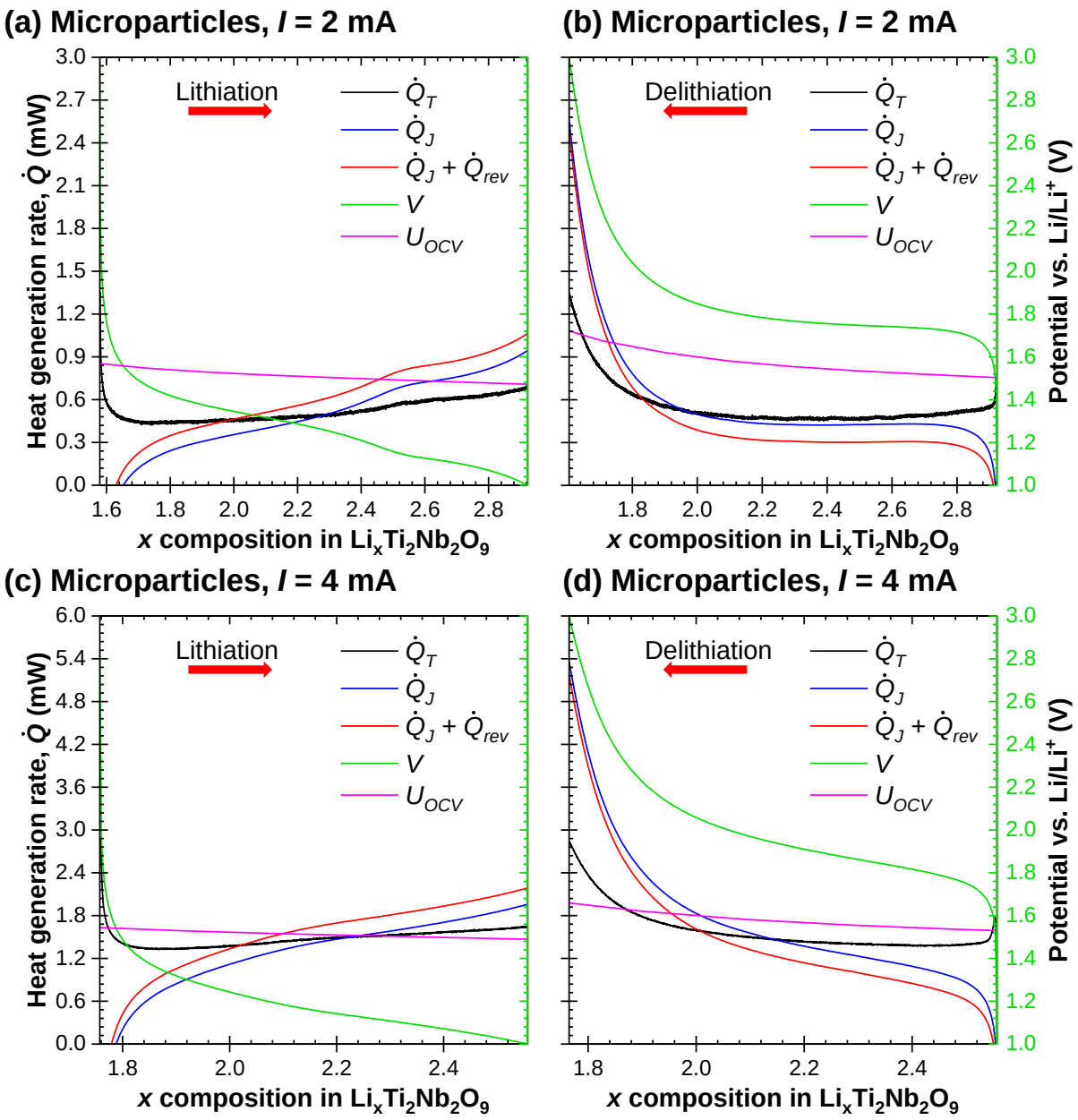

Figure S6: Measured total heat generation rate $\dot{Q}_T(x,T)$, along with heat generation rates $\dot{Q}_J(x,T)$ and $\dot{Q}_J(x,T) + \dot{Q}_{rev}(x,T)$ calculated according to Equations (5) and (6) in Manuscript, as well as measured cell potential $V(x,T)$ and open-circuit voltage $U_{OCV}(x,T)$ as functions of lithium composition x during (a) lithiation, (b) delithiation at current $I = 2$ mA, (c) lithiation, (d) delithiation at current $I = 4$ mA in calorimetric cell with working electrode made of $Ti_2Nb_2O_9$ microparticles and lithium metal counter electrode.

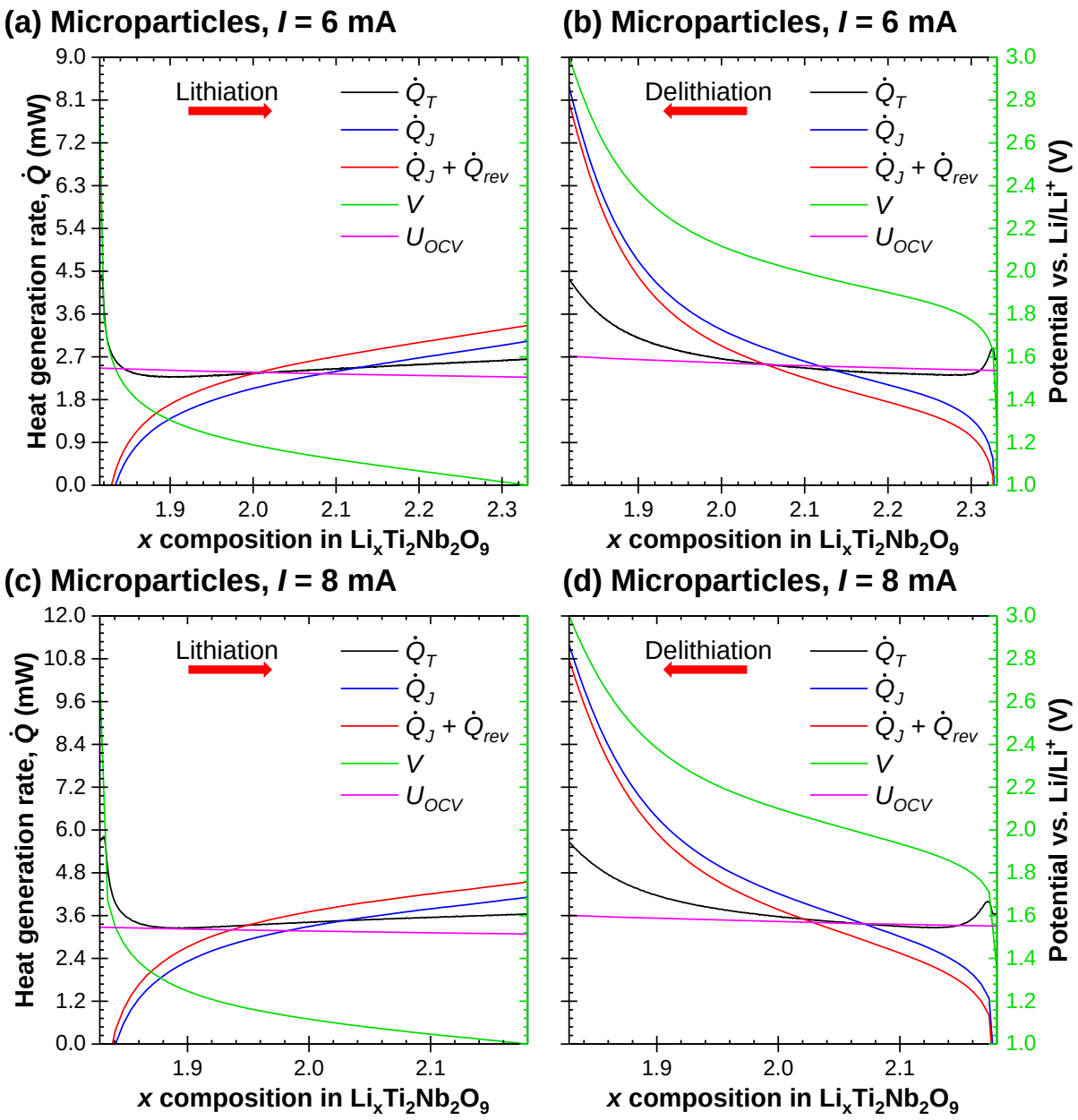

Figure S7: Measured total heat generation rate $\dot{Q}_T(x,T)$, along with heat generation rates $\dot{Q}_J(x,T)$ and $\dot{Q}_J(x,T) + \dot{Q}_{rev}(x,T)$ calculated according to Equations (5) and (6) in Manuscript, as well as measured cell potential $V(x,T)$ and open-circuit voltage $U_{OCV}(x,T)$ as functions of lithium composition x during (a) lithiation, (b) delithiation at current I = 6 mA, (c) lithiation, (d) delithiation at current I = 8 mA in calorimetric cell with working electrode made of $Ti_2Nb_2O_9$ microparticles and lithium metal counter electrode.

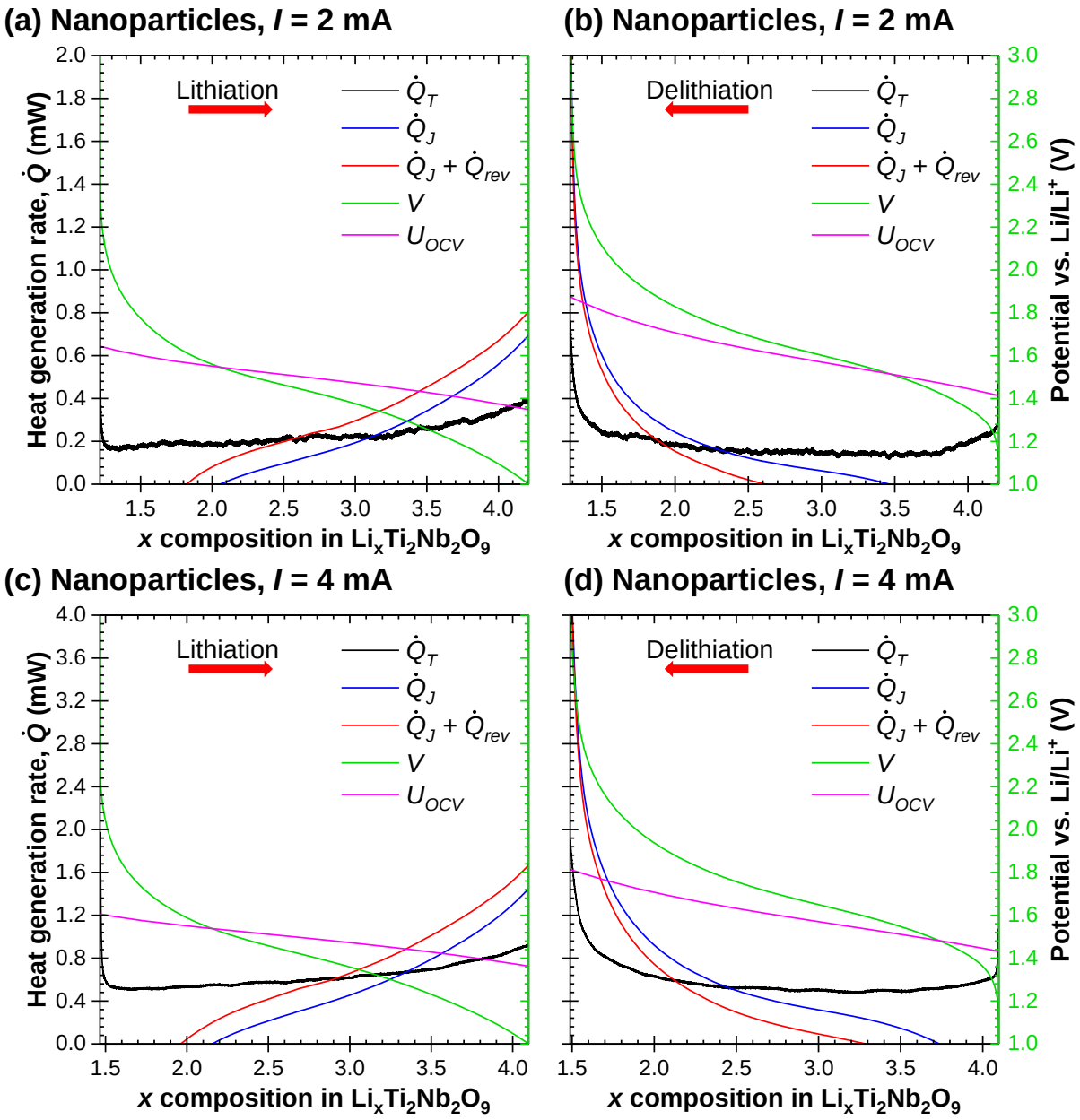

Figure S8: Measured total heat generation rate $\dot{Q}_T(x,T)$, along with heat generation rates $\dot{Q}_J(x,T)$ and $\dot{Q}_J(x,T) + \dot{Q}_{rev}(x,T)$ calculated according to Equations (5) and (6) in Manuscript, as well as measured cell potential $V(x,T)$ and open-circuit voltage $U_{OCV}(x,T)$ as functions of lithium composition x during (a) lithiation, (b) delithiation at current $I = 2$ mA, (c) lithiation, (d) delithiation at current $I = 4$ mA in calorimetric cell with working electrode made of $Ti_2Nb_2O_9$ nanoparticles and lithium metal counter electrode.

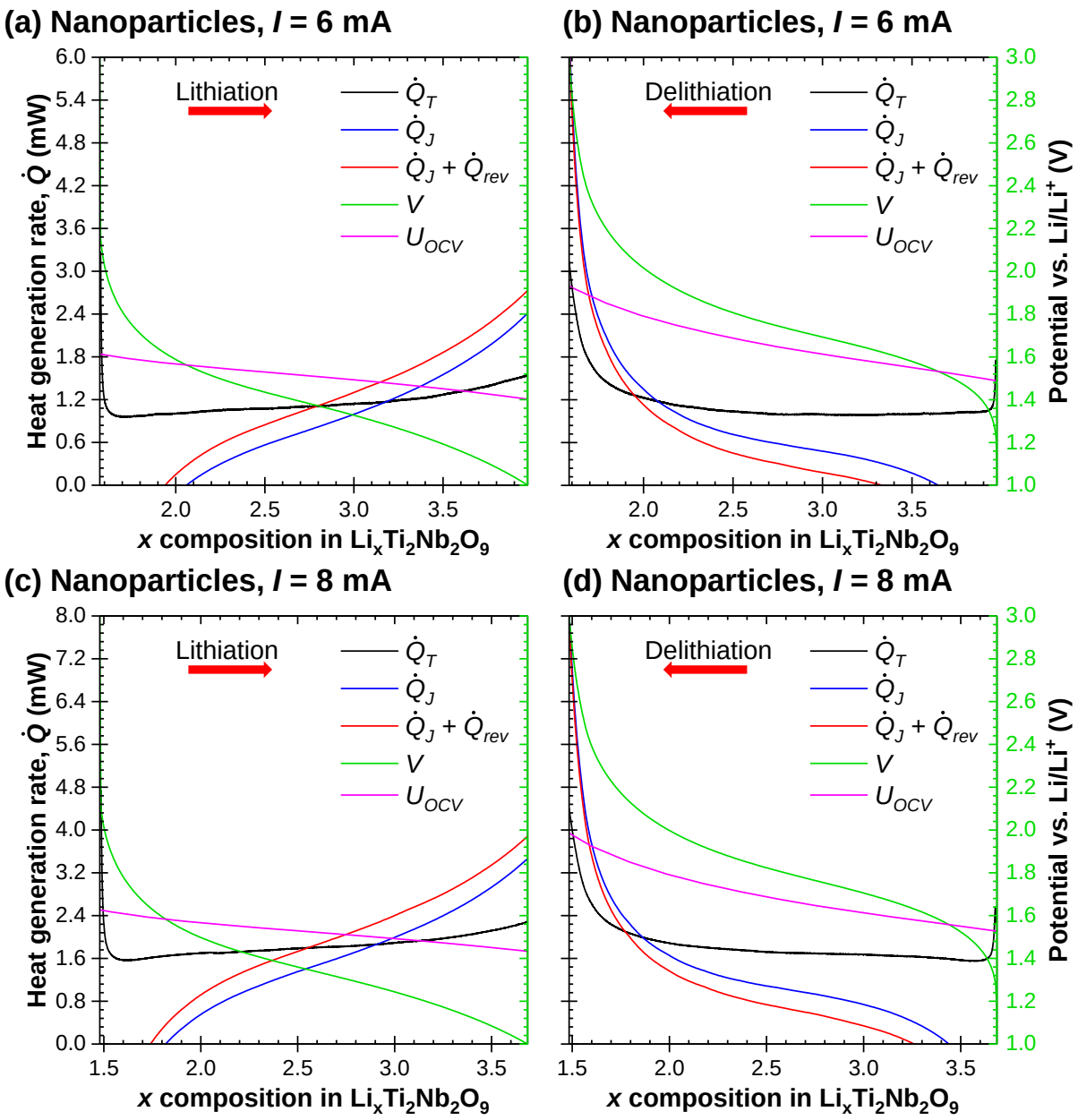

Figure S9: Measured total heat generation rate $\dot{Q}_T(x,T)$, along with heat generation rates $\dot{Q}_J(x,T)$ and $\dot{Q}_J(x,T) + \dot{Q}_{rev}(x,T)$ calculated according to Equations (5) and (6) in Manuscript, as well as measured cell potential $V(x,T)$ and open-circuit voltage $U_{OCV}(x,T)$ as functions of lithium composition x during (a) lithiation, (b) delithiation at current $I = 6$ mA, (c) lithiation, (d) delithiation at current $I = 8$ mA in calorimetric cell with working electrode made of $Ti_2Nb_2O_9$ nanoparticles and lithium metal counter electrode.

References

[1] S. W. Baek, K. E. Wyckoff, D. M. Butts, J. Bienz, A. Likitchatchawankun, M. B. Preefer, M. Frajnkovič, B. S. Dunn, R. Seshadri, and L. Pilon, "*Operando* calorimetry informs the origin of rapid rate performance in microwave-prepared $TiNb_2O_7$ electrodes", *Journal of Power Sources*, vol. 490, pp. 229537, 2021.

[2] S. W. Baek, M. B. Preefer, M. Saber, K. Zhai, M. Frajnkovič, Y. Zhou, B. S. Dunn, A. Van der Ven, R. Seshadri, and L. Pilon, "Potentiometric entropy and *operando* calorimetric measurements reveal fast charging mechanisms in PNb_9O_{25}", *Journal of Power Sources*, vol. 520, pp. 230776, 2022.